RAPID COMMUNICATIONS

PHYSICAL REVIEW B VOLUME 32, NUMBER 11 1 DECEMBER 1985

Near-surface defect profiling with slow positrons: Argon-sputtered Al(110)

A. Vehanen, J. Mäkinen, P. Hautojärvi, H. Huomo, and J. Lahtinen
Laboratory of Physics, Helsinki University of Technology, SF-02150 Espoo, Finland

R. M. Nieminen and S. Valkealahti
Department of Physics, University of Jyväskylä, SF-40100 Jyväskylä, Finland
(Received 30 May 1985)

We report on slow-positron measurements of atomic defect distribution near a solid surface. Defects are produced by argon-ion bombardment of an Al(110) surface in ultrahigh vacuum. Defect profiles have a typical width of 15–25 Å and contain a broader tail extending to 50–100 Å. The defect density at the outermost atomic layers saturates at high argon fluences to a few atomic percent, depending on sputtering conditions. Defect production rate at > 1 keV Ar^+ energies is typically 1–5 vacancy-interstitial pairs per incident ion. Molecular-dynamics simulations of the collision cascade predict similar defect distributions.

Low-energy ion bombardment of solid surfaces is extensively used for sample preparation and modification in surface science and technology.[1] While the yield and distribution of sputtered atoms and ions have been widely studied, and implantation profiles of the projectile atoms can be measured,[2] little is known about production and distribution of point defects and their agglomerates after low-energy particle irradiation.[3-5] Defects have a major effect on near-surface material properties, and their annealing after irradiation is often prerequisite for surface science experiments.

We have developed an experimental method to obtain quantitative information on the distribution of defects near a solid surface. In this Rapid Communication we demonstrate it to measure defect profiles in aluminum after argon-ion bombardment under various conditions. The method is based on detecting the probability J of a thermalized positron to diffuse back to the surface, as a function of the positron implantation energy E. The positron mobility is affected[6] by lattice defects, which can trap a freely diffusing positron, thus reducing J. The shape of J vs E curves is analyzed to yield spatial distribution of the vacancy-type defects, which are capable to trap positrons.

Also the annihilation characteristics of positrons inside the sample are affected by ion bombardment, as demonstrated by Triftshäuser and Kögel in He-irradiated nickel sample.[7]

The experimental facility is a variable-energy ($E=0$ to 30 keV) positron beam[8] with a base pressure of 3 nPa. Monoenergetic positrons (2×10^6 sec^{-1}, $\delta E \leq 4$ eV) strike the solid target and rapidly thermalize with a fairly well-known implantation profile $P(z,E)$,[6] having a shape close to a derivative of a Gaussian function.[9] A subsequent diffusive motion of the positron results in (i) positron annihilation from the delocalized (freely diffusing) state, (ii) trapping and annihilation at a defect site inside the sample, and (iii) diffusion back to the surface with a probability J.[10,11] A variety of processes take place upon the positron returning to the surface, e.g., formation and emission of an orthopositronium (o-Ps) atom.[10] Since o-Ps can only annihilate via 3γ emission (contrary to all other positron states, which disintegrate by 2γ emission[6]), J can be readily obtained by measuring the $3\gamma/2\gamma$ ratio with a Ge detector.[11,12]

The Al(110) sample[13] was prepared in a conventional way, which included a heating up to 800 K and (at later stages) sputtering with low-energy Ar^+. It was analyzed with low-energy electron diffraction and retarding field Auger-electron spectroscopy measurements. A characteristic low-energy electron-diffraction pattern was found and Auger-electron spectroscopy showed $\lesssim 1\%$ of a monolayer C and trace O contamination. The pressure throughout the experiments was < 20 nPa. Ar^+ sputtering was performed with $\sim 10\ \mu A/cm^2$ ion current in the energy range 0.1–3 keV and incident angle θ from 0° (normal) to 75°. After each sputtering $J(E)$ was measured.

From the measured back diffusion probability $J(E)$ we calculate the quantity[14]

$$K(E) = 1 - J_{\rm def}(E)/J_{\rm bulk}(E) , \qquad (1)$$

where $J_{\rm bulk}$ and $J_{\rm def}$ are results from samples before (no defects) and after sputtering, respectively. Thus $K\ (0 \leq K \leq 1)$ is a measure of the relative fraction of positrons trapped by lattice defects. Figure 1 shows examples of K vs E curves after bombarding with various Ar^+ energies

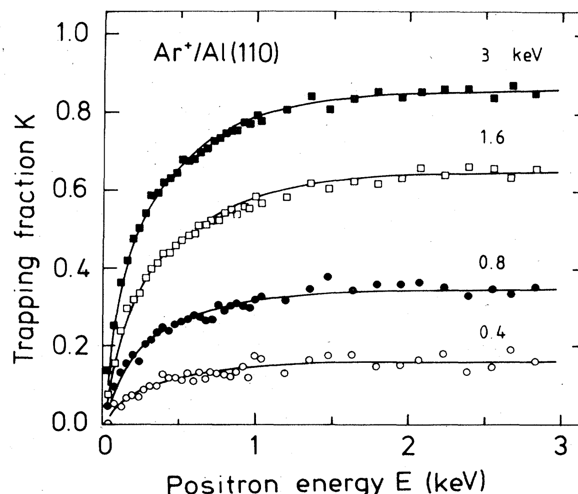

FIG. 1. Experimental positron trapping fractions K as a function of the positron implantation energy E in Al(110) single crystal after argon-ion bombardment. The Ar^+ fluence was $\sim 10^{17}$ cm^{-2} and the incident angle $\theta = 75°$. Ion energies are indicated in the figure. The solid lines are best fits to the positron diffusion-annihilation equation in the presence of a spatial defect distribution.

 ©1985 The American Physical Society

at an incident angle $\theta=75°$. The curves have been measured under conditions (Ar^+ fluence $\gtrsim 5\times10^{16}$ cm^{-2}), where the trapping fraction $K(E)$ becomes independent of the Ar^+ fluence. Obviously this corresponds to a dynamic equilibrium,[4] where the yield of sputtered atoms and the net production rate of the irradiation-induced defects are equal. The trapping fraction K in Fig. 1 increases strongly at low E and approaches a constant level at $E\sim1$ keV. This value of K corresponds to high-energy positrons, which are implanted far beyond[15] the defected overlayer. Consequently, they have an overall (independent of E) probability to diffuse through the damaged region to the surface. Thus the value of K at $E>1$ keV is a rough measure of the total number of defects,[16] while the shape of K vs E contains information on the shape of the defect distribution.

To obtain detailed knowledge on defect profiles we have fitted the $K(E)$ data to solutions of the quasistationary[17] diffusion-annihilation equation for the positron density $n(z,E)$:

$$D_+\nabla^2 n(z,E)-\lambda_b n(z,E)-\mu c(z)n(z,E)+P(z,E)=0 \ . \tag{2}$$

Here, D_+ ($=0.5$ cm^2/sec) is the positron diffusion coefficient, λ_b ($=6$ $nsec^{-1}$) annihilation rate of a free positron, μ the specific trapping rate into defects,[6] and $c(z)$ the defect concentration profile. We have solved[18] Eq. (2) by iteration: The profile $c(z)$ is first guessed and $n(z,E)$ is calculated numerically. Since $J(E)$ is proportional to the positron diffusion current emerging from the surface

$$J(E)=|-D_+\nabla n(0,E)| \ , \tag{3}$$

properly normalized values of $K(E)$ can be obtained from Eq. (1). Finally, $c(z)$ is varied until best fit to the data is found. The profiles were parametrized in terms of a Gaussian function followed by an exponential tail. The fits to the experimental data are shown as solid lines in Fig. 1, and they have typical χ^2 values ranging from 0.9 to 1.2.

The fitted K vs E curves are[18] rather independent of the parameters in the fitting procedure, e.g., coefficients describing the implantation profile $P(z,E)$.[9] By virtue of its definition [Eq. (1)], K is also rather insensitive to the uncertainties in measuring $J(E)$ from the $3\gamma/2\gamma$ ratio (*o*-Ps fraction).[12] The resulting profiles $c(z)$ typically contain a narrow (~15 Å) peak near the surface followed by a broader shoulder extending down to 50–100 Å.

Figure 2 shows the total number of defects per unit area and the mean depth of defects for samples sputtered at room temperature with a high Ar^+ fluence of varying energy with incident angles of $\theta=45°$ and 75°. We chose the specific trapping rate in Eq. (2) to be $\mu=5\times10^{14}$ sec^{-1}, which is the value found[6] for monovacancies in Al. Because vacancies in aluminum can migrate freely at room temperature,[19] the defects expected to trap positrons are small two- and three-dimensional vacancy clusters and vacancy-argon complexes.[20] Since μ is expected to be proportional to the number of vacancies in a small cluster,[21] our choice of μ is therefore a measure of the total number of vacancies associated with the sputtering-damage cascades.

The total number of defects per unit area depicted in Fig. 2 depends strongly on the sputtering energy and angle, whereas the mean depth of defects, $\langle z\rangle$, has a much weaker dependence on sputtering conditions. The integrated defect density in Fig. 2 increases linearly with Ar^+ energy, in

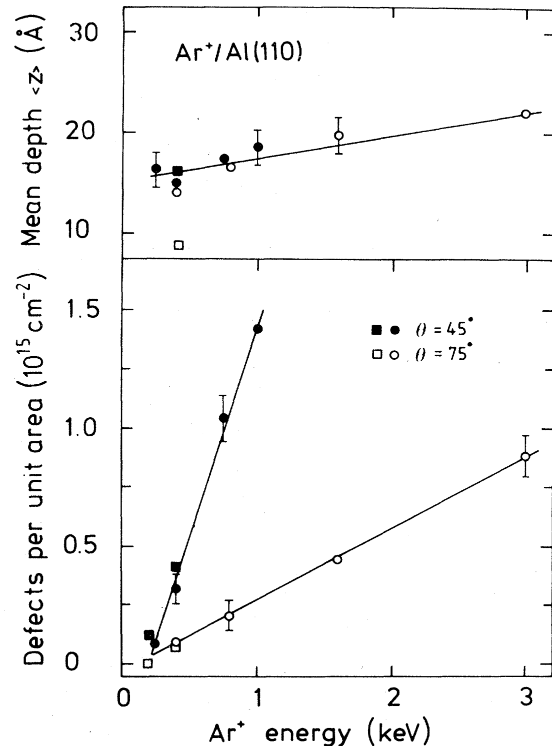

FIG. 2. Experimental (circles) and simulated (squares) characteristics of defect profiles in argon-bombarded Al(110) as a function of the Ar^+ energy at two different incident angles. The integral of the defect distribution (defects per unit area) and the mean depth of the profile $\langle z\rangle$ are shown. The integrals of the simulated vacancy profiles are scaled by a constant factor.

agreement with the classical model of Kinchin and Pease.[22] Defect production is negligible below Ar^+-ion energies of around 150 eV. Values of the total number of defects (per unit area) typically correspond to about one empty atomic layer, while the local defect concentration in the outermost layers is of the order of a few atomic percent. The latter value is characteristic for the density of vacancy-type defects in amorphous metals.[23]

To gain more insight into the generation of atomic defects during low-energy sputtering, we have simulated the sputtering damage with full-scale molecular-dynamics computer calculations.[18] The substrate was a (110) film of 70 layers of Al atoms interacting via (Morse) pair potentials. The parameters of the potential were chosen to give a correct (bulk) cohesion energy, compressibility and lattice constant. Periodic lateral boundary conditions were imposed on the basic computational unit cell containing 1400 atoms. The sputtering particle (Ar^+) with a chosen energy and incident angle was allowed to strike the surface. The Ar-Al potential was of the Moliere form.[24] The trajectories of the projectile and substrate atoms were calculated in discrete time steps ($\Delta t\approx10^{-15}$ sec). To allow for electronic slowing down, friction terms of the form $dE/dz=-k_iE^{0.5}$ were introduced into the equations of motion of the atoms, i.e., electronic slowing down proportional to ion velocities[25] was assumed. Values for k_i were adapted from a recent[26] calculation both for Ar and Al ions moving in metallic Al. The simulation continued until all the atoms had slowed down

below the displacement threshold of about 10 eV. To account for short-term recovery, a recombination radius of 4 Å for vacancy-interstitial pairs was assumed in analyzing the damage distribution. All other vacancies were included in counting the defect profiles for various sputtering conditions. The resulting integral and mean depth $\langle z \rangle$ of the calculated profiles are shown for some cases in Fig. 2. (squares). The agreement with the experimental data is good, although the calculated profiles tend to be shallower at very low Ar^+ energies and high-incident angles.

Figure 3 shows a typical profile $c(z)$, determined both experimentally and theoretically, which corresponds to an Ar^+ energy of 400 eV and incident angle of $\theta = 25°$. The simulated vacancy profile has a pronounced peak at the outermost layers with a tail extending to 100 Å. The shape of the simulated profile is in satisfactory agreement with the experimentally deduced distribution. The simulated interstitial atom profiles (not shown) have a relatively lower peak near the surface. The calculated sputtering yield is 0.8 atoms/Ar^+, which is also in good agreement with the measured low-energy yields.[1]

The simulated defect production rate (400 eV, 25°) is about six vacancy-interstitial pairs per each Ar^+ ion. The simulated vacancy profile results from a single Ar^+ ion,[27] whereas the experiments are done at an equilibrium state[4] ($\sim 10^{17}$ Ar^+/cm^2), where the defect profile is independent of the Ar^+ fluence. Therefore the integrals of the profiles in Figs. 2 and 3 cannot be directly compared to the experiments. Consequently, we have used a constant scaling factor for the simulated defect densities in Fig. 2. We have also performed measurements with use of lower Ar^+ fluences. The defect production rate during 750 eV argon sputtering at $\theta = 45°$ was estimated to be around three vacancy-type defects per incident ion. Comparison of these results with the computations allows us to get a rough idea of the long-term recombination probability, which obviously is responsible for the smaller areas of the experimentally deduced defect profiles.

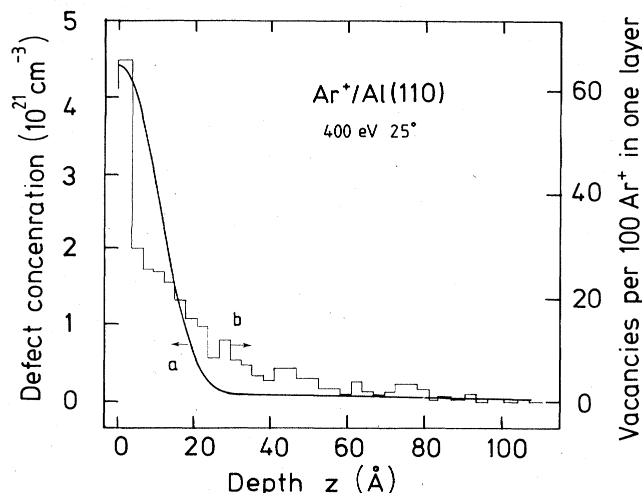

FIG. 3. (a) Experimental and (b) simulated defect profiles in Ar^+-sputtered Al(110). The experimental Ar fluences ($\sim 10^{17}$ cm^{-2}) correspond to a regime of dynamic equilibrium, where the profiles are fluence independent. The simulations are performed with 100 incident Ar^+ ions. Each bar in the graph includes two lattice planes.

In conclusion, we have for the first time obtained quantitative information on atomic-scale defect distribution near a single-crystal surface. An Al(110) surface sputtered with low-energy argon ions contains up to a few atomic percent vacant lattice sites at the outermost layers, and the defect distribution extends down to 50–100 Å. The method utilizing the unique properties of slow positron beams can be extended to analyze similar problems associated, e.g., with interfacial disorder, overlayer structures, and defects in multilayer components. Such work is currently in progress.

[1] *Sputtering by Particle Bombardment I*, edited by R. Behrisch, Topics in Applied Physics, Vol. 47 (Springer-Verlag, New York, 1981).
[2] A. Zomorrodian, S. Tougaard, and A. Ignatiev, Phys. Rev. B **30**, 3124 (1984).
[3] R. Miranda and J. M. Rojo, Vacuum **34**, 1069 (1984).
[4] L. K. Verheij, J. A. Van den Berg, and D. G. Armour, Surf. Sci. **122**, 216 (1982).
[5] B. Poelsema, L. K. Verheij, and G. Comsa, Phys. Rev. Lett. **53**, 2500 (1984).
[6] *Positrons in Solids*, edited by P. Hautojärvi, Topics in Current Physics, Vol. 12 (Springer-Verlag, New York, 1979); *Positron Solid State Physics*, edited by W. Brandt and A. Dupasquier (North-Holland, Amsterdam, 1983).
[7] W. Triftshäuser and G. Kögel, Phys. Rev. Lett. **48**, 1741 (1982).
[8] A. Vehanen, J. Lahtinen, H. Huomo, J. Mäkinen, and P. Hautojärvi, in *Positron Annihilation*, Proceedings of the Seventh International Conference on Positron Annihilation, New Delhi, 6-11 January 1985, edited by P. C. Jain, M. R. Singru, and K. P. Gopinathan (World Scientific, Singapore, 1985).
[9] S. Valkealahti and R. M. Nieminen, Appl. Phys. A **32**, 95 (1983).
[10] A. P. Mills, Jr., Phys. Rev. Lett. **41**, 1828 (1978).
[11] K. G. Lynn and D. O. Welch, Phys. Rev. B **22**, 99 (1980).
[12] P. J. Schulz, K. G. Lynn, and H. H. Jorch, in *Proceedings of the International Workshop on Slow Positrons in Surface Science, Pajulahti, Finland, June 1984*, edited by A. Vehanen, Laboratory of Physics Report No. 135, 1984 (Helsinki University of Technology, Helsinki, Finland).
[13] Kominco Co., purity 99.9999+%, mosaic spread < 0.2°, residual resistivity ratio > 40.000.
[14] A. Vehanen, J. Mäkinen, P. Hautojärvi, and P. Huttunen, in Ref. 8.
[15] The mean positron penetration depth $\bar{z}$ varies in aluminum as $\bar{z} = 145$ Å $(E/\text{keV})^{1.6}$; see Ref. 10.
[16] More specifically, the level of K at $E > 1$ keV is related to the integrated defect density weighted with the distance measured from the surface, viz. $\int_0^\infty c(z) z\, dz$, see Ref. 18.
[17] R. M. Nieminen, J. Laakkonen, P. Hautojärvi, and A. Vehanen, Phys. Rev. B **19**, 1397 (1979).
[18] J. Mäkinen, A. Vehanen, P. Hautojärvi, H. Huomo, J. Lahtinen, R. M. Nieminen, and S. Valkealahti (unpublished).
[19] R. W. Balluffi, J. Nucl. Mater. **69&70**, 240 (1978).
[20] Small interstitial agglomerates are not expected to act as positron traps, see, e.g., Ref. 6.
[21] R. M. Nieminen and J. Laakkonen, Appl. Phys. **20**, 181 (1979).
[22] G. H. Kinchin and R. S. Pease, Rep. Prog. Phys. **18**, 1 (1955).
[23] A. Vehanen, K. G. Lynn, P. J. Schultz, E. Cartier, H.-J. Güntherodt, and D. M. Parkin, Phys. Rev. B **29**, 2371 (1984).
[24] C. Varelas, and J. Biersack, Nucl. Instrum. Methods **79**, 213 (1970).
[25] E. Fermi and E. Teller, Phys. Rev. **72**, 399 (1947).
[26] M. J. Puska and R. M. Nieminen, Phys. Rev. B **27**, 6121 (1983).
[27] In the simulations, the irradiation damage is calculated and counted after each incident Ar^+ ion, whereafter a perfect lattice is resumed.